Journal of Molecular Structure 1233 (2021) 130054

Contents lists available at ScienceDirect

Journal of Molecular Structure

journal homepage: www.elsevier.com/locate/molstr

Chemical growth dynamics of 4-Methyl-4′-Hydroxy Benzylidene Aniline NLO single crystal structure and spectroscopic applications

R. Sakunthaladevi[a,b], L. Jothi[c,*]

[a] Department of Physics, Trinity College for Women, Namakkal, 637002, India
[b] Periyar University, Palkalai Nagar, Salem, 636011, Tamil Nadu, India
[c] Department of Physics, Namakkal Kavignar Ramalingam Government Arts College for Women, Namakkal, 637001, Tamil Nadu, India

ARTICLE INFO

Article history:
Received 24 December 2020
Revised 23 January 2021
Accepted 31 January 2021
Available online 9 February 2021

Keywords:
Crystal structure
X-Ray Diffraction
Single crystal growth
Organic compounds
Nonlinear optical materials

ABSTRACT

An aromatic Schiff bases organic nonlinear optical single crystal of 4-methyl-4′-hydroxy benzylidene aniline (MHBA) was grown by slow evaporation solution growth technique and the solubility of MHBA in ethanol at increasing temperature was esteemed. The unit cell proportions were gained by both single crystal and powder X-ray diffraction analysis. The structural refinement of MHBA shows that it crystallizes in the orthorhombic system with space group P_{bcn}. The molecule chiefly consists of two non – planar benzene rings attached by carbon and nitrogen atoms. The various planes of reflection were identified from the powder X-ray diffraction study and the unit cell proportions were same for single crystal XRD. Functional assemblies were entrenched by using Fourier transform infrared and FT Raman analysis by the molecular vibrations in the MHBA crystal. The assignment of protons and carbons in the grown MHBA crystals were recognized from ^{1}H and ^{13}C Nuclear Magnetic Resonance Spectroscopy analyses. The UV- visible and fluorescence spectral evaluate were carried out and to find the optical transmission and emission range of MHBA. The second harmonic generation productivity of MHBA is about 1.04 times than that of a standard sample of potassium dihydrogen orthophosphate. The thermal constancy of the grown crystal was investigated by differential scanning calorimetric, thermo gravimetric and a differential thermal analysis which confirms the decomposition of the sample occurs at 120 °C. Mechanical stuff, the hardness number, yield strength and Young's modulus of the grown material were studied using Vickers micro hardness tester and the work hardening coefficient reveals that MHBA belongs to the family of soft materials. The dielectric measurements with frequency and temperatures were used to find the power dissipation of the grown MHBA crystals.

1. Introduction

Studies on the design and synthesis of molecular materials with larger hyper-polarizabilities have become a hot research topic in current years because of their high optical nonlinearity [1–3]. Materials that display high optical nonlinearity find potential applications in devices for optical communications, optical processors, wavelength filters, modulators, data storage and optical switches [4]. Nonlinear optical (NLO) materials usually used in optical switching, optical data storage for the embryonic technologies in telecommunications, frequency mixing, optical parametric oscillation, optical bi-stability, optical logic gates, laser radiation protection, optical image processing, under water communication, biomedical, signal processing analysis, etc. [5]. The NLO properties of organic materials depend on their molecular level inside the material. The reallocate of dipolar environment initiates the electrochemical switching of the second-order NLO response at the molecular level [6]. Aromatic organic NLO materials are charming a great deal of attention for possible uses in optical devices because of their large optical nonlinearity, low cutoff wavelength, short response time and high laser damage thresholds [7]. Several organic materials showing considerable NLO effects have been identified and synthesized. However, only a rare of them could be crystallized and explored for a second order or third order NLO applications. Significant work has been done to understand the microscopic origin of the nonlinear behavior of organic aromatic materials [8–10]. Any compounds of the type Ar-CH=N-Ar ('Ar' is the aromatic ring formation) called Schiff bases exhibit large second order

* Corresponding author.
E-mail address: jothilakshmanan@gmail.com (L. Jothi).

https://doi.org/10.1016/j.molstruc.2021.130054
0022-2860/

NLO properties due to their thermochromism and photochromism [11]. Condensation of primary amines with aldehydes or ketones yields Schiff bases containing imine (C=N) functional group of the above type [12]. The benzylidene aniline derivatives are such kinds of materials and it is obvious material for the incredible transmitter of green light and form a good stable crystal [13]. Its derivatives exhibit conformational changes due to the rotation along the longest molecular axis, and consequently the molecules result in dynamic disorder in their crystal structures [14]. Also, benzylidene aniline derivatives are referred to as imines, anils, azomethines, Schiff bases, etc. due to the presence of C=N pond. The linkage of H-C=N in the certain reactions prompted us to design noncentrosymmetric class for the application of quadratic nonlinear optical effects [15].

Some of the following benzylidene derivatives 4-methoxy-4′-dimethylamino benzylidene aniline [16], 4-chloro-4′-bromo benzylidene aniline [17], 4-nitro-4′-methyl benzylidene aniline [18] and Metal doped 4-chloro-4′-bromo benzylidene aniline [19] are already reported and exhibit NLO properties higher than KDP. The titled compound 4-methyl-4′-hydroxy benzylidene aniline is a new aromatic imine compound with molecular formula $C_{14}H_{13}NO$. It crystallizes in the orthorhombic system in the chiral space group Pbcn with two independent molecules in the asymmetric unit. The type of crystalline space group to have a dependence on the non-linear optical properties of the materials [20]. So in this article, we account for the material synthesis, growth, structure, optical, thermal, mechanical, and dielectric and NLO properties of 4-methyl-4′-hydroxy benzylidene aniline single crystal.

2. Experimental details

2.1. Material synthesis

The title compound was synthesized by condensation reactions between 4-hydroxy benzaldehyde (*p*-HB) and 4-methyl aniline (*p*-MA) taken in the equimolar ratio. The basic compounds of high purity are purchased from Sigma Aldrich and used without purification.The reaction combination was relaxed in ethanol for about 8 hour, and the solution was filtered and the resulting product of 4-methyl-4′-hydroxy benzylidene aniline (MHBA) was obtained as a colorless crystalline powder. The reaction mechanism is described in Scheme 1. The synthesized salt was purified from ethanol by a successive recrystallization process.

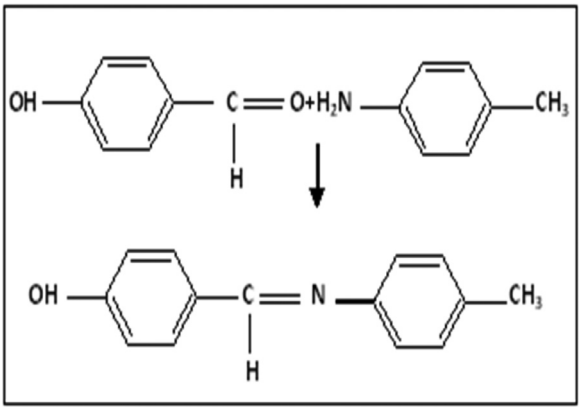

Scheme 1. Reaction mechanism of MHBA.

2.2. Growth of MHBA crystal

Re-crystallized salt was dissolved in ethanol and the solution was maintained at the desired temperature, and stirred continuously to ensure homogenization of the solution. On attainment, the saturation, the quantity of the salt in the solution was estimated gravimetrically. The same practice was repetitive at the temperatures of 30 °C to 55 °C with an increase of 5 °C and the results are shown in Fig. 1. The solubility graph undoubtedly states that the solubility directly increases with the increase in temperature. The 4-methyl-4′-hydroxy benzylidene aniline exhibits good solubility and positive solubility with temperature incline in ethanol.

Single crystals of 4-methyl-4′-hydroxy benzylidene aniline were grown by slow evaporation at room temperature. About 250 ml of saturated solutions was equipped at room temperature and it was carefully filtered using Whatman filter paper of pore size 11 μm. The filtered solution was reserved in a beaker, which was tightly closed for controlling a solvent slow evaporation [21]. Transparent neutral single crystal of dimension 20 × 20 × 2.5 mm^3 was harvested in an evolutionary period of seven days and the grown crystal is shown in Fig. 2.

Fig. 3

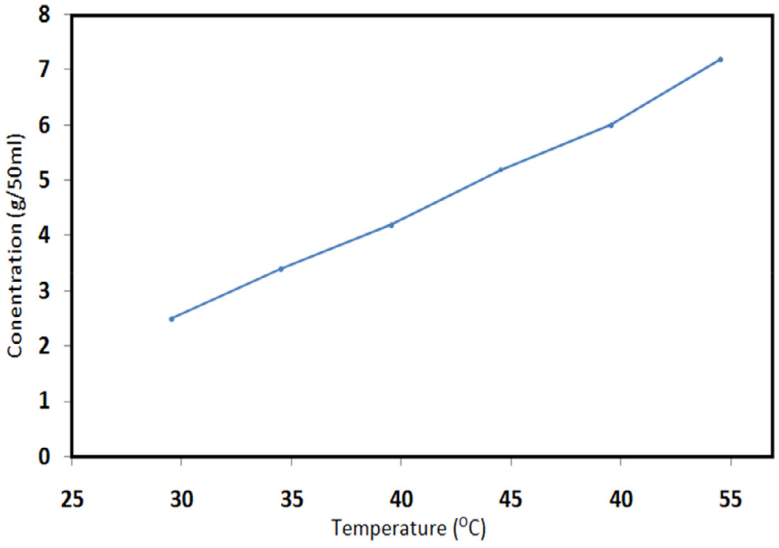

Fig. 1. Solubility curve of MHBA.

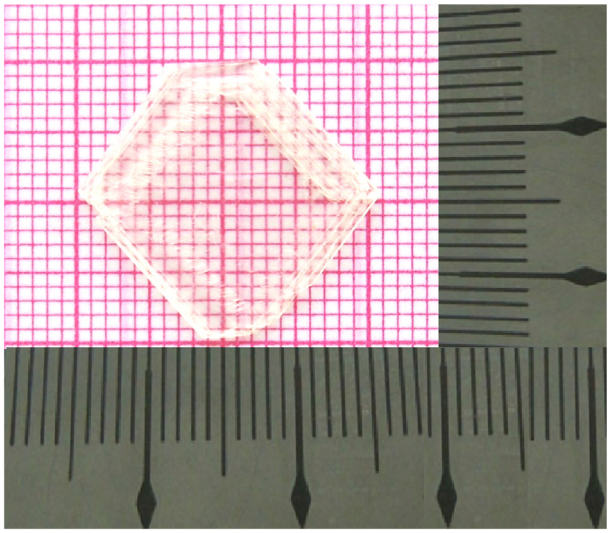

Fig. 2. As grown single crystal of MHBA.

3. Results and discussions

3.1. Single crystal X-ray diffraction

Single crystal X-ray diffraction analysis was performed on the as grown MHBA crystal using Enraf-Nonius CAD-4. The concentration data of the title compound were collected at 293 K on an SAD-ABS [22] system using MoKa (λ = 0.71073 Å) graphite monochromatic radiation. Crystal data and enhancement details are canned in Table 1.

The atomic coordinates and the selected bond distances are listed in Tables 2 and 3. The molecular assembly of MHBA was refined by the least-squares method using anisotropic displacement parameters specified in Table 4. The compound crystallizes in an orthorhombic crystal system with a Pbcn space group. The parameter values intended are a = 21.6180(10) Å, b = 11.0561(6) Å, c = 9.3318(5) Å and Z = 8.

Table 1
Crystal data and structure refinement for MHBA.

Empirical formula	C_{14} H_{13} N O
Formula weight	211.25 g/mol.
Temperature	293(2) K
Wavelength	0.71073 Å
Crystal system, space group	Orthorhombic, Pbcn
Unit cell dimensions	a = 21.6180(10) Å alpha = 90 deg. b = 11.0561(6) Å beta = 90 deg. c = 9.3318(5) Å gamma = 90 deg.
Volume	2230.4(2) Å ^{3}
Z	8
Calculated density	1.258 Mg/m^3
Absorption coefficient	0.079 mm^{-1}
F(000)	896
Crystal size	0.30 × 0.20 × 0.20 mm
Theta range for data collection	3.01 to 25.00 deg.
Limiting indices	$-25 \le h \le 22$, $-13 \le k \le 13$, $-9 \le l \le 11$
Reflections collected	11,344
Unique Reflections	1961 [R(int) = 0.0283]
Completeness to theta = 25.00	99.9%
Absorption correction	Semi-empirical from equivalents
Max. and min. transmission	0.971 and 0.923
Refinement method	Full-matrix least-squares on F^2
Data / restraints / parameters	1961 / 0 / 148
Goodness-of-fit on F^2	1.075
Final R indices [I>2sigma(I)]	R_1 = 0.0356, wR_2 = 0.0900
R indices (all data)	R_1 = 0.0500, wR_2 = 0.0999
Extinction coefficient	0.0028(10)
Largest diff. peak and hole	0.190 and −0.139 eÅ^{-3}

The value of important hydrogen co-ordinates and torsion angles in Tables 5 and 6. From the ORTEP scheme of the MHBA molecule, it contains two phenyl rings bridged by a C=N imino moiety, the planes of which are disposed at an angle of 49.40(5°), screening significant deviation of the molecule from planarity as observed in similar assemblies [23–25]. The C9-C8-N1-C5 = 171.11(13°) torsion angles indicates that the terminal phenyl rings are twisted relative to the plane in which the C=N binary bond lies. The C9-C8 [1.451(2) Å] and N1-C5 [1.4221(19) Å] distances confirm π-electron delocalization between the benzene rings and the molecule can be observed as a partially delocalized π electron system.

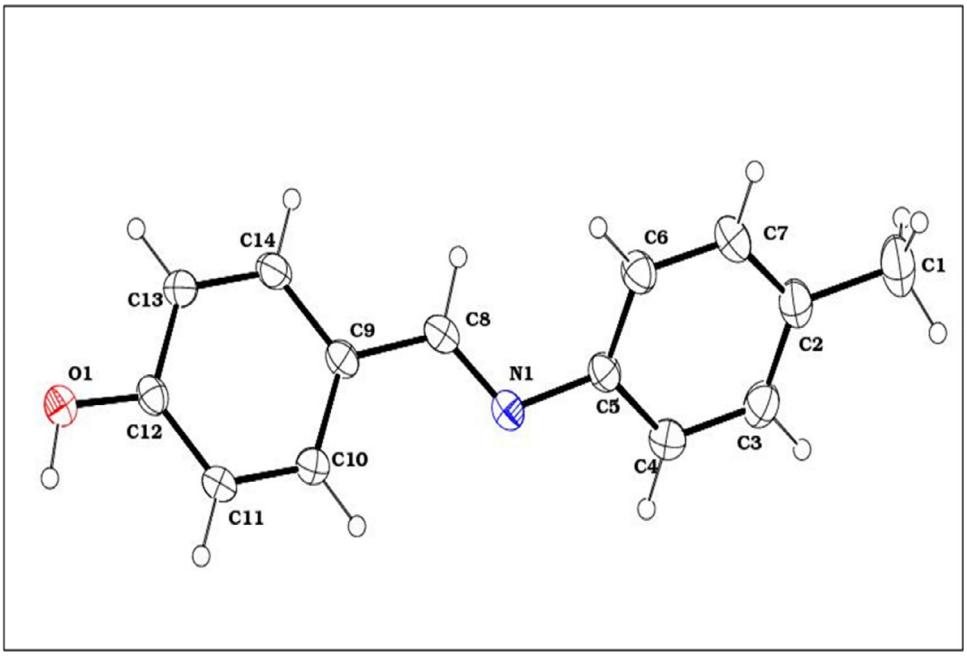

Fig. 3. ORTEP plot of MHBA.

Table 2
Atomic coordinates (x 10^4) and equivalent isotropic displacement parameters ($Å^2 \times 10^3$) for MHBA. U (eq) is defined as one third of the trace of the orthogonalized Uij tensor.

Atoms	x	y	z	U(eq)
C(1)	9840(1)	−3138(2)	5166(2)	70(1)
C(2)	9443(1)	−2257(2)	4351(2)	46(1)
C(3)	9387(1)	−1070(2)	4797(2)	48(1)
C(4)	9021(1)	−257(1)	4060(2)	42(1)
C(5)	8686(1)	−621(1)	2876(2)	34(1)
C(6)	8751(1)	−1801(1)	2398(2)	43(1)
C(7)	9123(1)	−2599(2)	3135(2)	48(1)
C(8)	7806(1)	−122(1)	1573(2)	36(1)
C(9)	7417(1)	613(1)	652(2)	34(1)
C(10)	7612(1)	1717(1)	84(2)	35(1)
C(11)	7251(1)	2347(1)	−872(2)	35(1)
C(12)	6684(1)	1891(1)	−1301(2)	34(1)
C(13)	6481(1)	797(1)	−740(2)	41(1)
C(14)	6843(1)	172(1)	215(2)	40(1)
N(1)	8305(1)	241(1)	2168(1)	35(1)
O(1)	6316(1)	2442(1)	−2270(1)	46(1)

Table 3
Bond distances and bond angles.

Moiety	Distance(Å)	Moiety	Angle(°)
C(1)-C(2)	1.504(2)	C(2)-C(1)-H(1A)	109.5
C(1)-H(1A)	0.9600	C(2)-C(1)-H(1B)	109.5
C(1)-H(1B)	0.9600	H(1A)-C(1)-H(1B)	109.5
C(1)-H(1C)	0.9600	C(2)-C(1)-H(1C)	109.5
C(2)-C(7)	1.382(2)	H(1A)-C(1)-H(1C)	109.5
C(2)-C(3)	1.383(2)	H(1B)-C(1)-H(1C)	109.5
C(3)-C(4)	1.381(2)	C(7)-C(2)-C(3)	117.54(15)
C(3)-H(3)	0.9300	C(7)-C(2)-C(1)	121.59(17)
C(4)-C(5)	1.381(2)	C(3)-C(2)-C(1)	120.87(17)
C(4)-H(4)	0.9300	C(4)-C(3)-C(2)	121.28(16)
C(5)-C(6)	1.387(2)	C(4)-C(3)-H(3)	119.4
C(5)-N(1)	1.4221(19)	C(2)-C(3)-H(3)	119.4
C(6)-C(7)	1.378(2)	C(3)-C(4)-C(5)	120.58(15)
C(6)-H(6)	0.9300	C(3)-C(4)-H(4)	119.7
C(7)-H(7)	0.9300	C(5)-C(4)-H(4)	119.7
C(8)-N(1)	1.279(2)	C(4)-C(5)-C(6)	118.63(14)
C(8)-C(9)	1.451(2)	C(4)-C(5)-N(1)	118.68(13)
C(8)-H(8)	0.9300	C(6)-C(5)-N(1)	122.66(14)
C(9)-C(14)	1.394(2)	C(7)-C(6)-C(5)	120.04(16)
C(9)-C(10)	1.396(2)	C(7)-C(6)-H(6)	120.0
C(10)-C(11)	1.375(2)	C(5)-C(6)-H(6)	120.0
C(10)-H(10)	0.9300	C(6)-C(7)-C(2)	121.84(16)
C(11)-C(12)	1.386(2)	C(6)-C(7)-H(7)	119.1
C(11)-H(11)	0.9300	C(2)-C(7)-H(7)	119.1
C(12)-O(1)	1.3496(18)	N(1)-C(8)-C(9)	124.80(14)
C(12)-C(13)	1.390(2)	N(1)-C(8)-H(8)	117.6
C(13)-C(14)	1.372(2)	C(9)-C(8)-H(8)	117.6
C(13)-H(13)	0.9300	C(14)-C(9)-C(10)	117.61(14)
C(14)-H(14)	0.9300	C(14)-C(9)-C(8)	119.57(13)
O(1)-H(1)	0.8811	C(10)-C(9)-C(8)	122.63(13)
		C(11)-C(10)-C(9)	121.17(13)
		C(11)-C(10)-H(10)	119.4
		C(9)-C(10)-H(10)	119.4
		C(10)-C(11)-C(12)	120.39(14)
		C(10)-C(11)-H(11)	119.8
		C(12)-C(11)-H(11)	119.8
		O(1)-C(12)-C(11)	123.45(14)
		O(1)-C(12)-C(13)	117.38(13)
		C(11)-C(12)-C(13)	119.16(14)
		C(14)-C(13)-C(12)	120.19(14)
		C(14)-C(13)-H(13)	119.9
		C(12)-C(13)-H(13)	119.9
		C(13)-C(14)-C(9)	121.47(14)
		C(13)-C(14)-H(14)	119.3
		C(9)-C(14)-H(14)	119.3
		C(8)-N(1)-C(5)	118.71(13)
		C(12)-O(1)-H(1)	109.5

Table 4
Anisotropic displacement parameters ($Å^2$ x 10^3). The anisotropicdisplacement factor exponent takes the form: $-2\ \pi^{\ 2}\ [h^2\ a^{*2}\ U_{11} + ... + 2\ h\ k\ a^*\ b^*\ U_{12}]$.

Atom	U11	U22	U33	U23	U13	U12
C(1)	60(1)	75(1)	74(1)	19(1)	−9(1)	19(1)
C(2)	39(1)	50(1)	49(1)	12(1)	3(1)	6(1)
C(3)	43(1)	57(1)	44(1)	4(1)	−7(1)	−4(1)
C(4)	45(1)	39(1)	43(1)	−2(1)	1(1)	−1(1)
C(5)	37(1)	33(1)	33(1)	4(1)	4(1)	1(1)
C(6)	50(1)	38(1)	40(1)	−2(1)	−3(1)	5(1)
C(7)	54(1)	38(1)	54(1)	1(1)	2(1)	11(1)
C(8)	43(1)	28(1)	38(1)	2(1)	7(1)	2(1)
C(9)	39(1)	29(1)	35(1)	−1(1)	4(1)	4(1)
C(10)	37(1)	32(1)	36(1)	−1(1)	2(1)	−1(1)
C(11)	42(1)	26(1)	37(1)	2(1)	3(1)	−1(1)
C(12)	39(1)	30(1)	35(1)	−3(1)	1(1)	7(1)
C(13)	36(1)	32(1)	54(1)	0(1)	−2(1)	−2(1)
C(14)	42(1)	28(1)	50(1)	5(1)	4(1)	−1(1)
N(1)	40(1)	32(1)	33(1)	1(1)	2(1)	4(1)
O(1)	48(1)	37(1)	52(1)	8(1)	−12(1)	−1(1)

Table 5
Hydrogen coordinates (× 10^4) and isotropic displacement parameters ($Å^2 \times 10^3$).

Atom	x	y	z	U(eq)
H(1A)	10,178	−2713	5605	104
H(1B)	9999	−3738	4519	104
H(1C)	9597	−3525	5894	104
H(3)	9599	−814	5610	58
H(4)	9001	544	4363	51
H(6)	8543	−2055	1578	51
H(7)	9160	−3390	2805	58
H(8)	7683	−915	1744	44
H(10)	7993	2033	359	42
H(11)	7389	3083	−1234	42
H(13)	6099	486	−1011	49
H(14)	6702	−561	578	48
H(1)	6475(4)	3149(17)	−2500(6)	55

The flared of the exocyclic angle O1-C12-C11 = [123.45(14°)] may be caused by steric collaboration between atoms H11 and H1 (H11....H1 = 2.3029(1) Å) [Fig. 4]. The N1-C8-C9 [124.80(14°)] is more than the normal value of 120°; this might be a sign of repulsion between the lone pair of electrons on N1 and H10 (N1...H10 = 2.6892(1) Å) attached to C10. The crystal structure is steadied by intermolecular O–H...N hydrogen bond linking the neighboring molecules into an infinite chain along the a-axis (Fig. 5).

3.2. Powder X-ray diffraction analysis

The grown crystal was characterized by powder X-ray diffraction using a Bruker D8 Advance, Germany instrument with Cu K_α radiation (λ = 1.5406Å). The sample was skimmed in the range 1° to 80° at a scan rate of 1°min^{-1} and the lattice parameters were calculated by the unit cell software program. Shrill peaks in the spectrum point to the good crystallinity of the grown crystal [26] which confirmed by the powder X-ray diffraction study of MHBA crystal. Peaks perceived from the X-ray diffraction spectrum (Fig. 6) were indexed and these standards approve well with the consistent values obtained from single crystal XRD.

3.3. Fourier Transform Infrared Spectral analysis

Fourier Transform Infrared spectrum of the grown MHBA crystal was recorded in the range 400 cm^{-1} - 4000 cm^{-1} using Perkin Elmer (Model RX1). The arranged sample was followed by the pressed KBr pellet technique. The FT-IR spectrum gives the vibra-

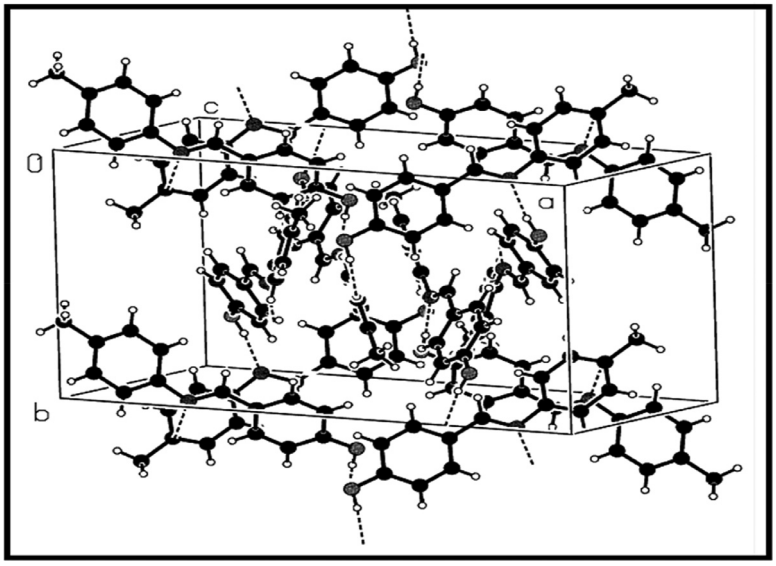

Fig. 4. The molecular arrangement in the unit cell.

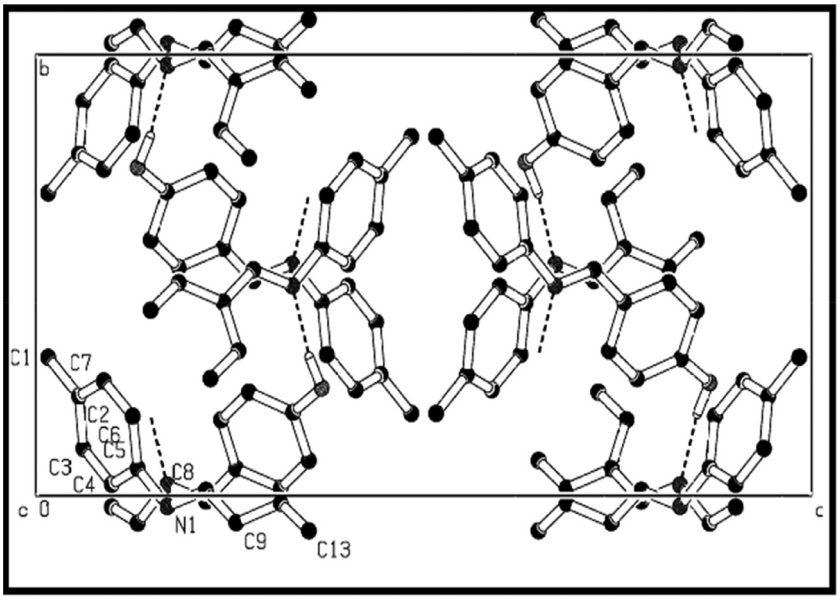

Fig. 5. A packaging diagram viewed along 'a' axis.

tional studies of the grown compound using infrared radiation and can provide the strong confirmation for the inter and intra molecular interaction occurrence in the compound as given in Fig. 7.

In the maximum of the benzylidene aniline results C=N stretching vibrations occurs nearly 1600 cm^{-1} caused by the formation of imine group [27]. In the MHBA spectrum, it was detected at 1592 cm^{-1} which confirms the presence of the imine group in the titled compound. The O–H stretching vibration was mostly observed in a range from 3200 cm^{-1} to 3570 cm^{-1} [28] in the MBHA peak obtained at 3410 cm^{-1}. Para-di-substituted benzenes display C–H deformation vibration in the region from 800 cm^{-1} to 840 cm^{-1} in this work appears at 828 cm^{-1} [18]. The bands found between 828 cm^{-1} and 530 cm^{-1} are due to C–H out of plane deformation [29]. Aldehyde distinctive band customarily present at 2720 cm^{-1} but the absence of which indicates the final product is not an aldehyde [30].

3.4. Investigation of Raman spectrum

The FT Raman spectrum of the MHBA was recorded on a BRUKER RFS 27 spectrometer equipped with an FRA 106 accessory in the region of 4000 cm^{-1} - 500 cm^{-1}. The spectrum in Fig. 8 gives the Raman scattering of molecules and the inelastic scattering of photons in a material. The Raman shift at 1575 cm^{-1} confirms the imine group (C=N) formation and also confirms the Raman activeness of imine group. Aromatic ring stretching vibration of C=C occurs for grown MHBA crystal is at 1444 cm^{-1}. The external modes which are due to translator and rotatory motion of molecules in the crystalline lattice have been appeared below 200 cm^{-1} [31].

The various peak values of characteristic FT Raman and FT IR are presented in Table 7. The vibrational bands pragmatic in both the spectra sustenance the structure of MHBA. Both FT IR and FT

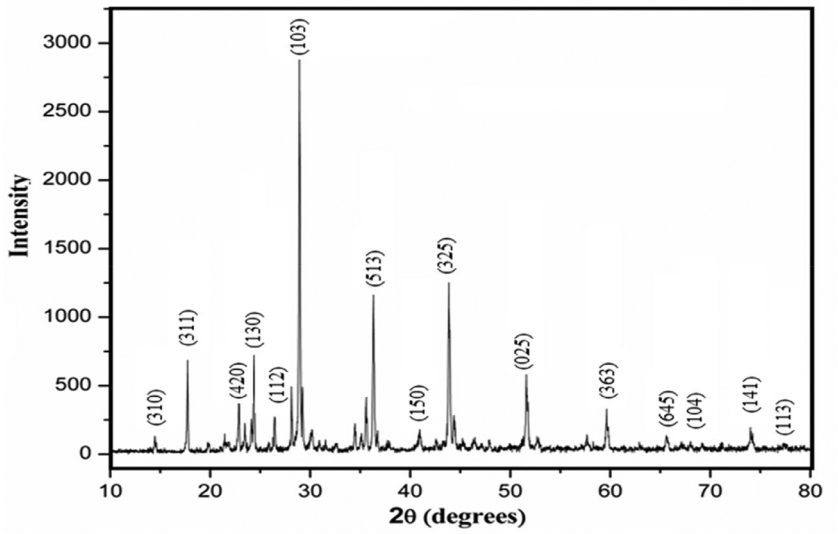

Fig. 6. Powder X-ray diffraction pattern of MHBA.

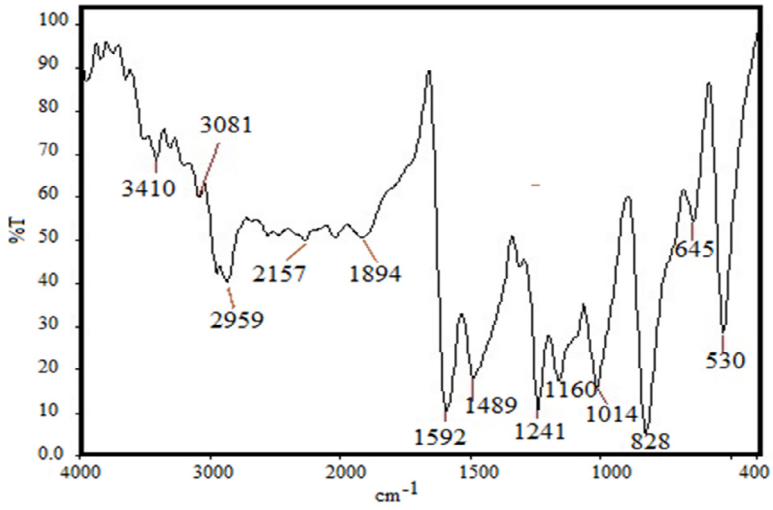

Fig. 7. FTIR spectrum of MHBA.

Raman spectroscopy are ideal methods for identification of molecular vibrations.

3.5. ^{1}H and ^{13}C NMR spectral analyses

The 300 MHz proton NMR spectrum of 4-methyl-4′-hydroxy benzylidene aniline measured in DMSO using Bruker instrument is integrated for a total of 10 protons. The recorded ^{1}H- NMR spectrum for MHBA is shown in Fig. 9. A triplet at 2.457 ppm is due to CH_3 protons. The vest at 9.979 ppm is dispensed to the hydroxyl group attached to the carbon in the benzene ring. The vest at 8.4 ppm is due to CH proton and a singlet at 8.404 due to the construction of the C=N imine group. The doublets at 7.307 ppm, 6.627 ppm, 7.806 ppm and 7.165 ppm correspond to the protons present in the benzene rings [32]. The compounds structure is further confirmed from its ^{13}C NMR spectrum. There are ten sets of carbon existing in the compound. Two correspondent carbonyl carbons C(3) and C(7) resonate at δ=130 ppm, equivalent C(4) and C(6) were reverberating at δ =129 ppm. Additional carbon resonance signals can be dispensed as C(10) and C(14) at δ =134 ppm, C(11) and C(13) at δ =134 ppm, C(9) at δ =151 ppm, C(12) at δ =143 ppm, C(8) at δ =161 ppm, C(5) at δ =123 ppm, C(12) at δ=117 ppm and C(1) at δ =77 ppm [33] all are shown in Fig. 10. The molecular structure of MHBA was verified by the carbon hydrogen bonded (C=H) network.

3.6. UV-VIS spectral studies

The optical transmission spectrum of MHBA single crystal was recorded in the region from 100 nm to 1100 nm using Perkin Elmer Lamda 35 spectrophotometer. It gives appreciated information about the structure of molecules because the absorption of UV and visible light involves the promotion of electrons in σ and π orbital from the ground state to a higher energy state [34]. The extreme transmittance is about 98% for MHBA crystal of 2 mm thickness and the lower cut-off wavelength is obtained at 219 nm. Fig. 11 displays that the crystal has a wide transparent opening in the UV, visible and infrared regions [35], in the range from 390 nm to 1100 nm, which point to that this crystal can be used as a potential material for SHG or other optical applications in the visible and NIR regions [36].

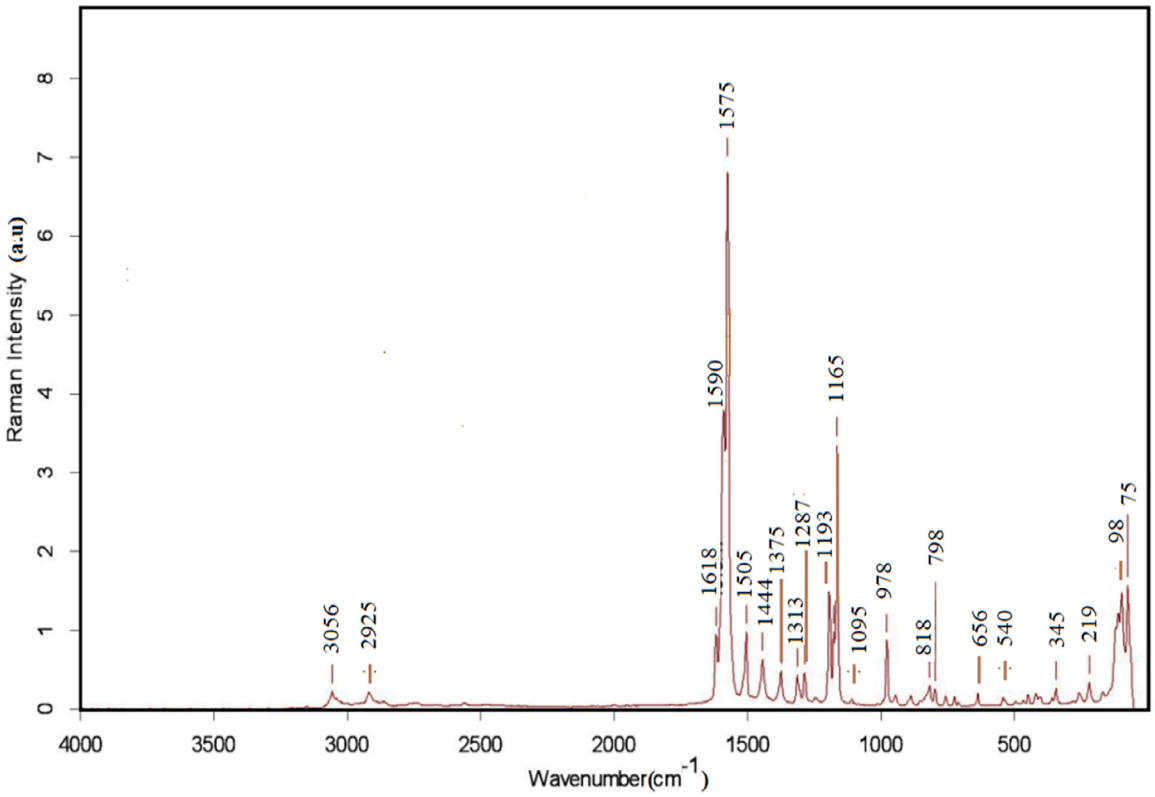

Fig. 8. FT-Raman spectrum of MHBA.

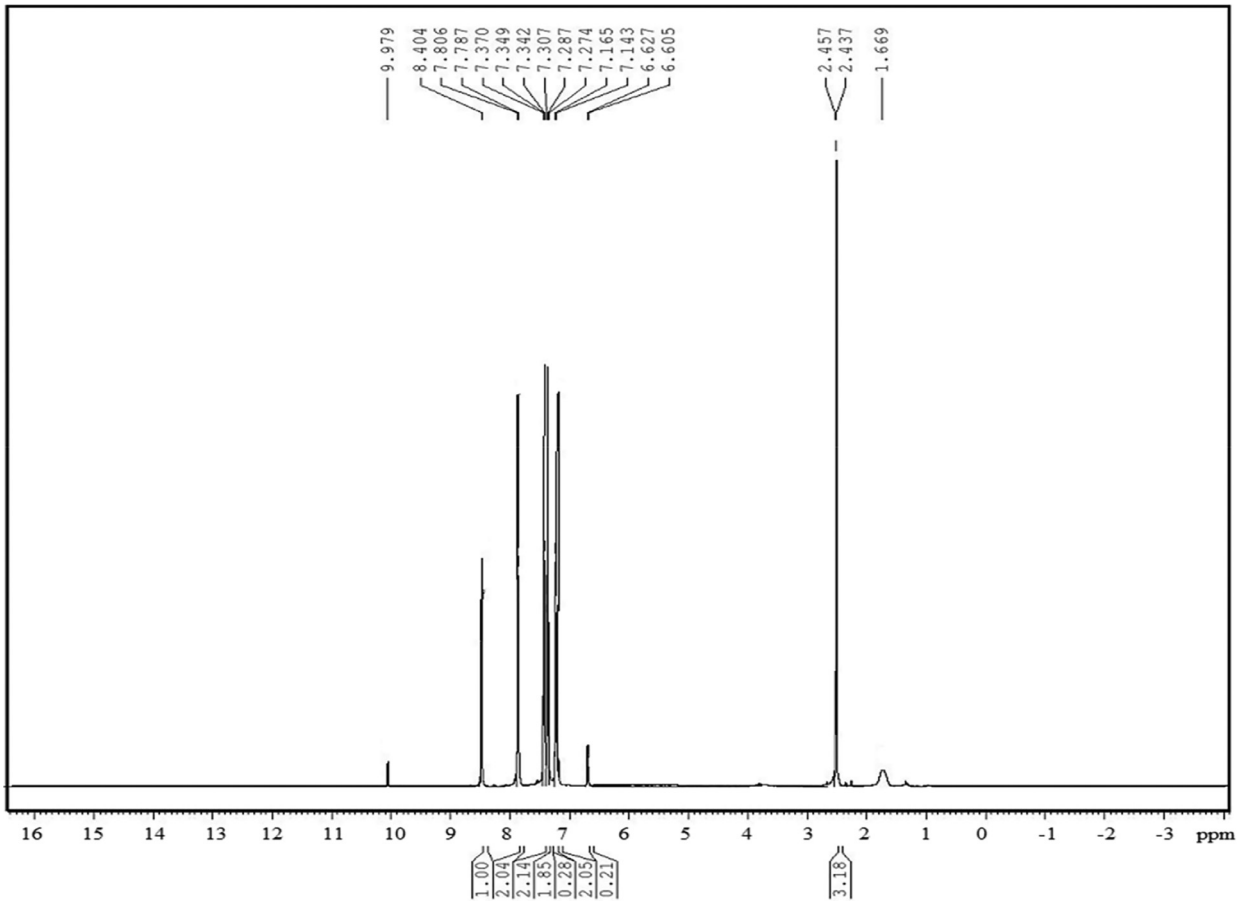

Fig. 9. ^{1}H - NMR spectrum of MHBA.

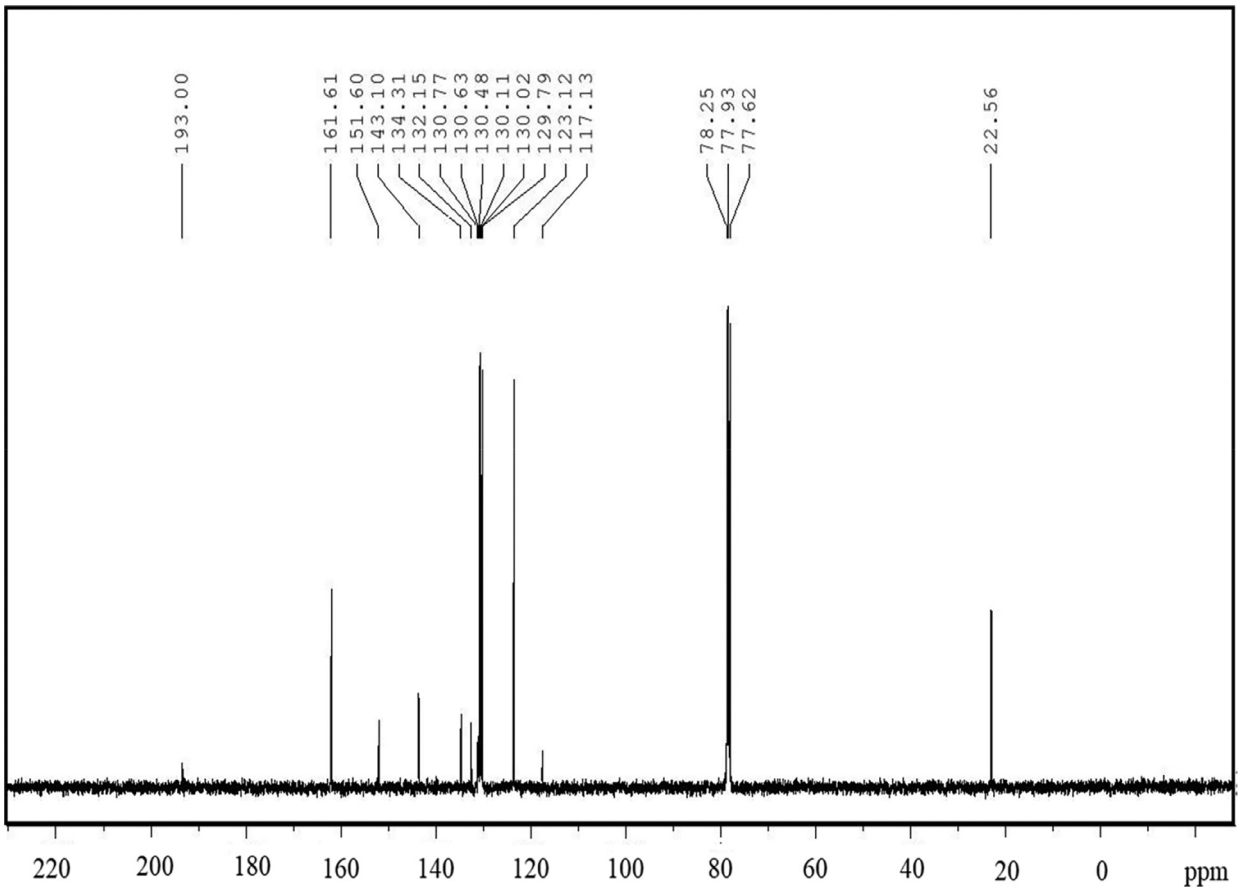

Fig. 10. ^{13}C NMR spectrum of MHBA.

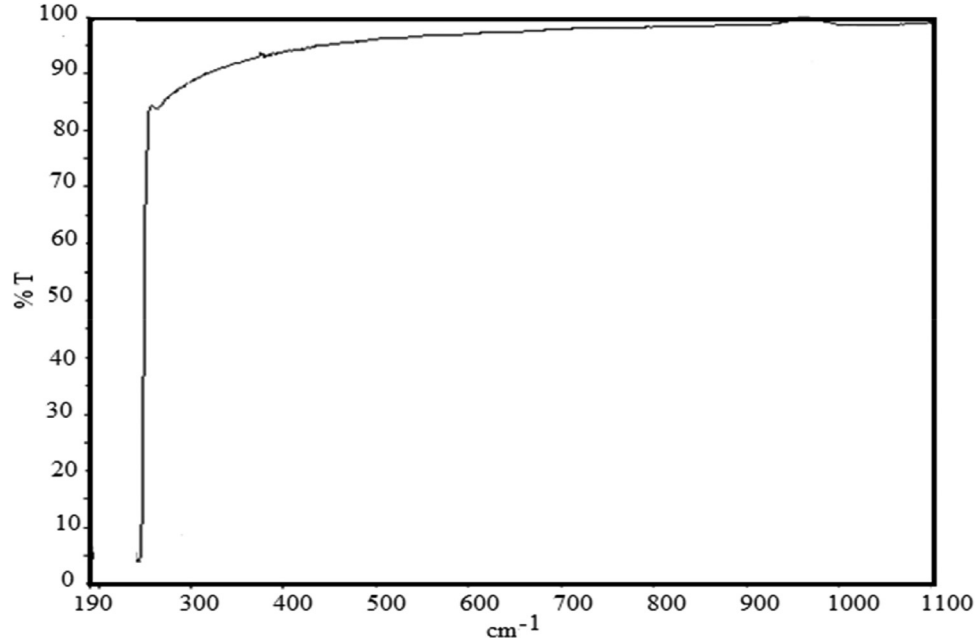

Fig. 11. UV–VIS Transmission spectrum of MHBA.

Table 6
Torsion angles [degrees].

C(7)-C(2)-C(3)-C(4)	0.3(3)
C(1)-C(2)-C(3)-C(4)	−179.72(16)
C(2)-C(3)-C(4)-C(5)	2.0(2)
C(3)-C(4)-C(5)-C(6)	−3.5(2)
C(3)-C(4)-C(5)-N(1)	178.62(14)
C(4)-C(5)-C(6)-C(7)	2.7(2)
N(1)-C(5)-C(6)-C(7)	−179.48(14)
C(5)-C(6)-C(7)-C(2)	−0.4(3)
C(3)-C(2)-C(7)-C(6)	−1.1(3)
C(1)-C(2)-C(7)-C(6)	178.95(17)
N(1)-C(8)-C(9)-C(14)	−171.69(15)
N(1)-C(8)-C(9)-C(10)	13.4(2)
C(14)-C(9)-C(10)-C(11)	−0.1(2)
C(8)-C(9)-C(10)-C(11)	174.95(14)
C(9)-C(10)-C(11)-C(12)	−0.3(2)
C(10)-C(11)-C(12)-O(1)	−177.82(13)
C(10)-C(11)-C(12)-C(13)	0.7(2)
O(1)-C(12)-C(13)-C(14)	177.90(14)
C(11)-C(12)-C(13)-C(14)	−0.7(2)
C(12)-C(13)-C(14)-C(9)	0.3(2)
C(10)-C(9)-C(14)-C(13)	0.1(2)
C(8)-C(9)-C(14)-C(13)	−175.12(14)
C(9)-C(8)-N(1)-C(5)	−171.11(13)
C(4)-C(5)-N(1)-C(8)	−147.79(14)
C(6)-C(5)-N(1)-C(8)	34.4(2)

The bandgap energy of a sample is premeditated by using the formula [37],

$$\mathrm{Eg} = \frac{1240}{\lambda}(\mathrm{nm})$$

where λ is lower cut off a wavelength in the UV – VIS transmission spectrum and the value obtained is 267 nm. Using the above formula, the calculated bandgap energy value of MHBA crystal is 4.6 eV. The optical transmission range and the transparency cutoff wavelength are essential for materials used in optoelectronic applications [38].

3.7. Fluorescence studies

Fluorescence may be expected generally in molecules that are aromatic or contain multiple conjugated double bonds with a high degree of resonance stability [39]. The excitation and emission spectra of the MHBA were recorded using JOBINVYON FLURO LOG 3 spectrofluorometer. The emission spectrum was restrained in the range 300 nm – 600 nm as shown in Fig. 12.

It is detected that the crystal was excited at 271 nm, the consistent emission was observed at 396 nm. In MHBA fluorescences are caused by carbonyl chromophore and the central C=N bond [40,41]. The optical band gap of MHBA is determined as 4.6 eV, which concurs well with the bandgap calculated from the UV-VIS optical transmission spectrum. Fluorescence finds extensive application in the branches of biochemistry, medicine and analytical tools and detection methods in material science [42].

3.8. SHG studies

The second harmonic generation (SHG) intensity of the grown crystals was recorded using Kurtz and Perry powder technique [43]. A Nd: YAG laser beam of a wavelength 1064 nm with pulses of 9 ns with the repetition rate of 10 Hz was used. The crystalline sample of MHBA and the reference sample of KDP were powdered to the particle size of ≈ 125 μm. The SHG intensity is subject to the particle size of the sample [44]. The release of green light with a power of 166.4 mV and 160 mV were measured for the MHBA and KDP correspondingly. The SHG efficiency of MHBA was found to be 1.04 times greater than that of KDP.

3.9. Thermal analyses

The grown MHBA crystal was subjected to Thermo Gravimetric Analysis (TGA) and Differential Thermal Analysis (DTA) and the spectra are shown in Fig. 13. They were documented using a simultaneous thermal analyzer TGA Q500 V20 in a nitrogen atmosphere for a temperature range from 30 °C to 600 °C 10 °C at a heating rate of 10°C/min. The decomposition switches nearly from 120 °C to 225 °C and a major weight loss of 99% obtained at 208°C. The weight loss directed that the decomposition nature of the sample and NLO applications MHBA was used below 120°C [45]. However, there is no weight loss was detected below 100 °C which shows there is no water molecule in MHBA [46].

A sharp exothermic peak at 121 °C was obtained in the DTA spectrum of MHBA which indicates the melting point of the grown sample. The weight loss was spotted at 121 °C from this the decomposition starts before melting. The acuity of the peaks indicates a good degree of crystallinity of the sample [47,48]. The differential scanning calorimetry (DSC) measurement of MHBA was carried by using a sample of 10 g with a thermal analyzer of Netzsch DSC 204. A DSC plot of MHBA crystal is exposed in Fig. 14. Very sharp endothermic peak detected at 121 °C with an area of 99 J/g well coincided with the TG-DTA spectrum of MHBA.

3.10. Vickers microhardness studies

Mechanical stuff on the grown MHBA crystal was tested by using the Vickers hardness indentor with varying load from 25 g to 100 g with constant indentation time of 10 s. The profile of the impression depends on the material, its structure and which face verified [49]. The hardness number H_V for the grown crystals can also be estimated by using the relation,

$$\mathrm{H_v} = \frac{1854P}{d^2}\left(\mathrm{Kgm^{-2}}\right)$$

where P is the applied load for testing in g and d is the diagonal length of the indentor used in mm [50]. The hardness number for various loads like 25 g, 50 g and 100 g are calculated by using the above formula and shown in Fig. 15. On the additional increase of

Table 7
FTIR and FT Raman band assignments of MHBA crystal.

FTIR (cm^{-1})	FT Raman (cm^{-1})	Assignments
3031	3056	C-H symmetric stretching
2985	2915	C-H stretching in CH_3
2867	2886	C-H asymmetric stretching
1592	1590	C=N stretching
1449	1444	C=C stretching in aromatic ring
1241	1287	Asymmetric and Symmetric deformation mode of methyl group
1160	1165	Aromatic– C-H plane bending
828	821	C-H bending mode
645	656	Out of plane bending of hydroxy group
530	540	**C–C** deformation

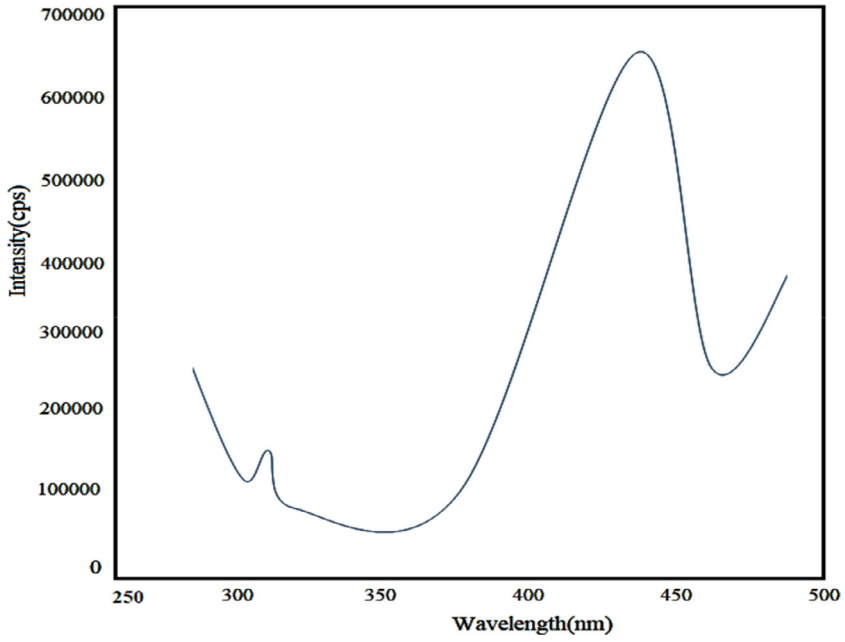

Fig. 12. Fluorescence spectrum of MHBA.

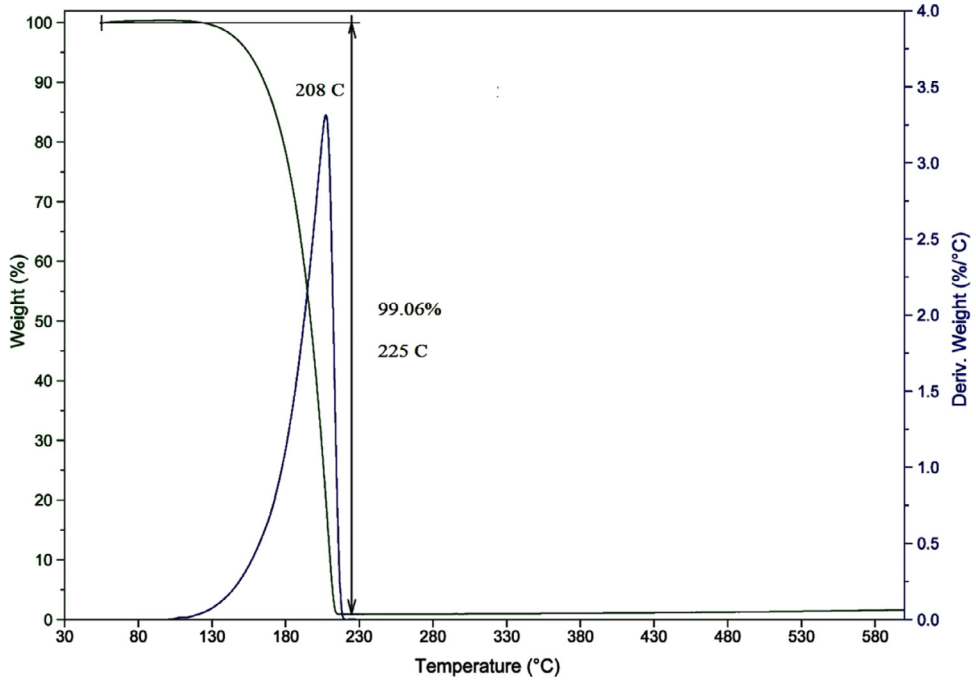

Fig. 13. TGA-DTA curve of MHBA.

the load beyond 100 g, cracks established on the surface of the crystal caused by the release of internal stress generated locally by indentation [51]. The C_{11} (elastic stiffness constant) was calculated from Hv by using the formula [37],

$$C_{11} = (H_v)^{7/4}(GPa)$$

there are two important aspects in determining the value of C_{11}. The opening aspect is the tightness of bonding between the neighboring atoms. The next aspect is the rate of variation with the position of the atoms of the forces of attraction and repulsion between them [52]. The elastic stiffness constant value of MHBA crystals for a load of 25 g is 14.10 GPa. The Young's Modulus describes the elastic properties of a solid undergoing tension or compression in only one direction otherwise called elastic modulus. Using the Vickers microhardness number, the Young's modulus of the crystal also calculated using the relation [53],

$$E = \left(\frac{0.45Hv}{0.1406 - \frac{b}{a}}\right)(Nm^{-2})$$

where b and a are the shorter and longer indentation diagonal lengths of the indentor impressed through the material. The elastic modulus is an intrinsic property of a material, up to a primary level E is a measure of the bond strength between the atoms in a material.

The greater the modulus, the stiffer the material but the value is 0.2540×10^{10} Nm^{-2} for a load of 25 g. The minimum value

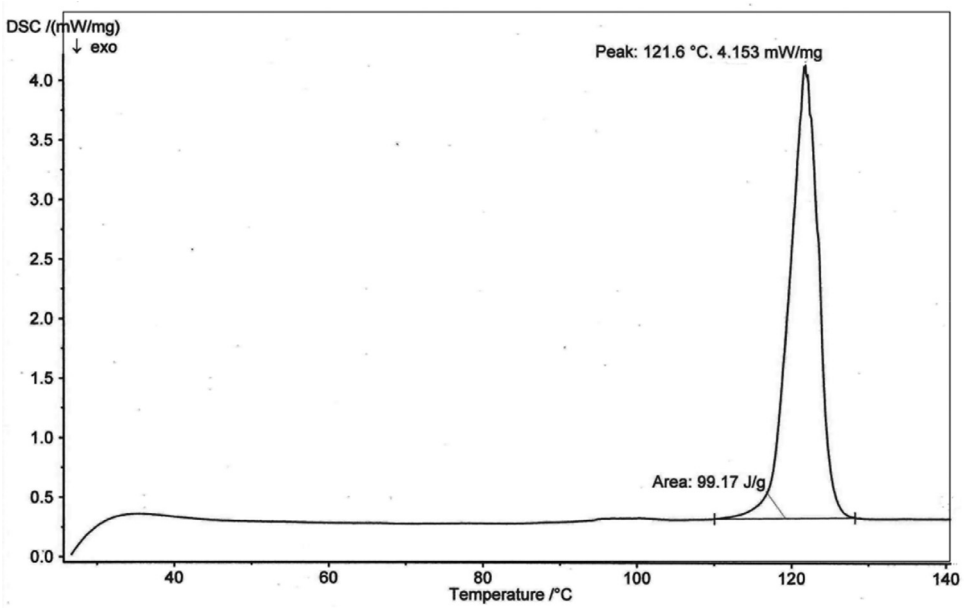

Fig. 14. DSC curve of MHBA.

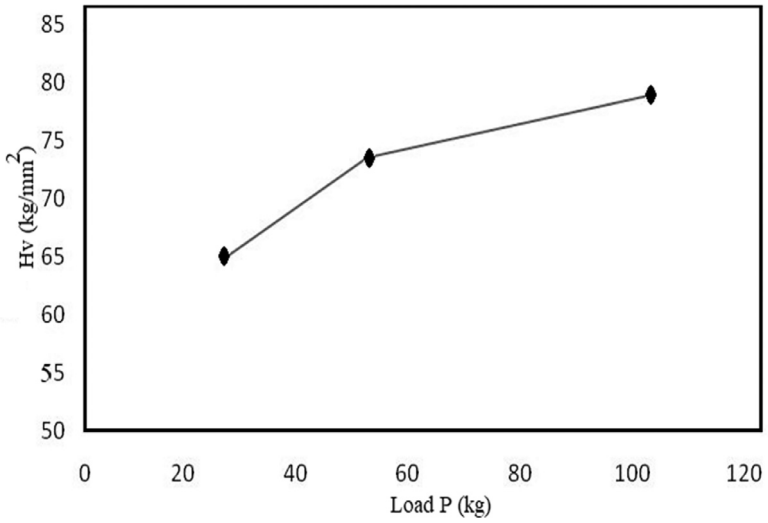

Fig. 15. Hardness Vs. Load for MHBA.

of Youngs modulus indicate that MHBA crystal an example of soft material. The Meyers index number or work hardening coefficient (n) is calculated from Meyers law by,

$$P = ad^n$$

the relation involving the applied load and diagonal length d of the indenter used for testing. It is also used to measure the mechanical strength of the materials, and that could be calculated from the slope of a straight line between log P and log d^2. Onitsch [54] and Hanneman [55] indicate that n lies between 1.0 and 1.6 for hard material and is more than 1.6 for soft materials. The work hardening coefficient is inverse to the hardness of the material [56]. The n value detected in the present studies is just around 2.583 signifying that MHBA crystals are moderately soft materials. Table 8 shows the comparison of microhardness number and work hardening index of MHBA with some organic crystals.

3.11. Dielectric studies

The dielectric properties normally correlate with the electro-optical property of crystals [63] and also provide information about the superiority of the materials [64]. The grown MHBA single crystal was subjected to dielectric studies using HIOKI 3532 - 50 LCR HITESTER impedance meter. The cut and polished surface of the sample was electrode with silver paste for electrical contact. The experiment was carried out for the frequencies from 0 Hz to 1 MHz with the temperatures of 30°C, 40°C, 50°C and 60 °C. In general, the dielectric response would be good in the lower region for the organic crystals. From the Fig. 16 to find that the dielectric constant decreases with increasing frequency at all measured temperatures. In low frequency nearly 500 kHz the value of a dielectric constant is very small of the order of 98 at temperature 30 °C but at temperature 60°C the dielectric constant is rise to 283. Also the frequency above 500 kHz the value of dielectric constant

Table 8
Comparison of microhardness number (H_v) and work hardening index (n).

Crystals	Crystal System	H_v	n	Reference
Benzamidazole	Orthorhombic	29	2.06	[57]
P- hydroxy acetophenone	Orthorhombic	25	2.04	[58]
4, 4′-dimethyl benzophenone	Orthorhombic	17.2	1.65	[59]
2 amino–5 chloro benzophenone	Monoclinic	23	1.50	[60]
L – Alanine triethanol amine	Orthorhombic	24	2.40	[61]
L – Alaninium maleate	Orthorhombic	64	1.65	[62]
4-methyl-4′-hydroxy benzylidene aniline	Orthorhombic	65	2.58	Present work

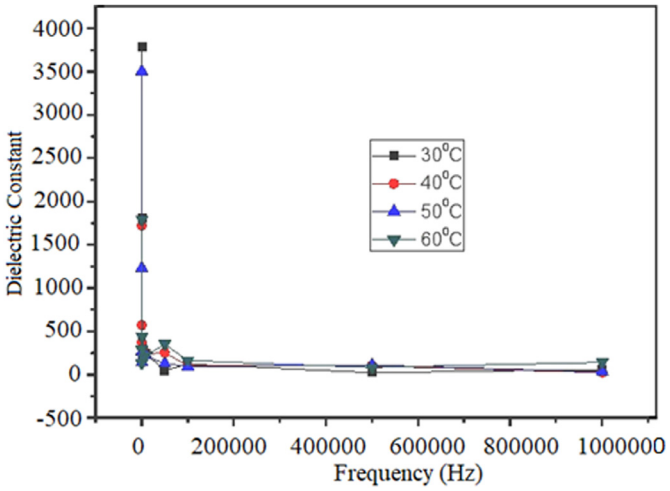

Fig. 16. Variation of a dielectric constant of MHBA as function of frequency at different temperatures.

changes gradually and above 1 MHz it attains nearly a saturation value at all the measured temperatures. The high values of ε_r at low frequencies might be caused by the presence of the four polarizations namely, space charge, orientational, ionic and electronic and its low value at high frequencies might be caused by gradual significance loss of these polarizations [65]. From the above results it is clear that the dielectric constant inversely depends on both the temperature and frequency. The dielectric constant was premeditated using the relation [66],

$$\varepsilon_r = \frac{Cd}{\varepsilon 0 A}$$

which relates the capacitance (F), thickness of the crystal used (m), vacuum dielectric constant (8.854×10^{-12} Fm^{-1}) and area of the crystal used (m^2).

The inverse association between a dielectric constant and frequencies is an important property for the fabrication of materials towards ferroelectric, photonic and electro-optic devices [67].

4. Conclusions

A new aromatic Schiff base organic NLO material of MHBA was synthesized by the condensation process and the solubility of MHBA was determined with an increase in temperature. The obtained MHBA single crystals were transparent and colorless with a dimension of $20 \times 20 \times 2.5$ mm^3. The intensity data of the MHBA crystal was recognized by the single-crystal X-ray analysis and the refinement details are summarized. The molecular structure of MHBA was refined by the least squares method and it crystallized into orthorhombic with P_{bcn} space group. This is compared with powder X-ray diffraction studies and confirmed the results obtained from single crystal XRD. In FT-IR spectra the peak near 1600 cm^{-1} confirmed the (C=N) stretching vibration in benzylidene aniline derivatives which is also confirmed by FT Raman spectral analyses. The consistent resonance frequency of the nuclei in a molecule is detected by ^1H and ^{13}C NMR spectra. It showed a peak at 193.8 in ^1H and 10.0 ppm in ^{13}C respectively of (HC=N) bonding, which was assigned to the azomethine carbon atom in the grown MHBA crystal. The optical transmission study exposed that the MHBA crystal was optically transparent in the entire visible and NIR region. The bandgap energy intended from UV-VIS and fluorescence spectrum is almost equivalent to 4.6 eV and it is an important parameter in optoelectronic applications. The second harmonic generation (SHG) efficiency was investigated to explore the nonlinear optical characteristics of the MHBA crystal, and it was 1.04 times that of KDP in green light emission. The thermal steadiness of the MHBA crystal nearly 120 °C which is confirmed by both the TG/DTA and DSC analyses. There is no weight loss below 100 °C which shows there is no water molecule in MHBA and the MHBA crystal is used below 120 °C in NLO applications. The mechanical strong point of the MHBA crystal was measured by Vickers micro hardness test and it shows reverse indentation size effect. The Young's modulus value and work hardening coefficient value of MHBA is 0.2540×10^{10} Nm^{-2} and 2.58 respectively and it directed that MHBA crystal belongs to soft material type. The dielectric behavior has been evaluated and testified as a function of frequency with rise in temperature. High values of a dielectric constant in low frequency for measured temperatures lead to more power dissipation of MHBA crystals.

Declaration of competing interest

The authors declare that they have no known competing financial interestsor personal relationships that could have appeared to influence the work reported in this paper.

Acknowledgements

One of the authors (LJ) thanks Sophisticated Instrumentation centre, Indian Institute of Technology, Chennai for the support in single crystal XRD, Fluorescence, DSC and TG/DTA data collection. LJ also, thanks to Prof. P.K. Das, Indian Institute of Science, Bangalore for having protracted laser facilities for SHG measurements and Central Electro Chemical Research Institute (CECRI), Karaikudi for NMR measures.

References

[1] A. Elmali, A. Karka, H. Unver, Chem. Phys. 309 (2005) 251–257.
[2] A. Karakas, A. Elmali, H. Unver, H. Kara, Y.Z. Yahsi, Naturforsch 61 (2006) 968–974.
[3] A. Karakas, H. Unvar, A. Elmali, J. Mol. Struct. 774 (2006) 67–70.
[4] S. Keinan, M.A. Ratner, T.J. Marks, Chem. Mater. 16 (2004) 1848–1854.
[5] M. Thairiyaraja, G. Arivazhagan, A. Elangovan, P. Anandan, G. Bakiyaraj, S.G. Praveen, K. Kirubavathi, K. Selvaraju, J. Nonlinear Opt. Phys. Mater. 27 (2018) 1850045–1850079.
[6] K. Clays, J. Nonlinear Opt. Phys. Mater. 12 (2003) 475–494.
[7] M.Narayan Bhat, S.M. Dharmaprakash, J. Cryst. Growth 236 (2002) 376–380.
[8] T. Suthan, N.P. Rajesh, J. Cryst. Growth 312 (2010) 3156–3160.
[9] Huaihong Zhang, Yu Sun, Xiaodan Chen, Xin Yan, Baiwang Sun, J. Cryst. Growth 324 (2011) 196–200.

[10] Natalia Zaitseva, Leslie Carman, Andrew Glen, Jason Newby, Michelle Faus, Sebastien Hamel, Nerine Cherepy, Stephen Payne, J. Cryst. Growth 314 (2011) 163–170.
[11] L. Jothi, R.Ramesh Babu, K. Ramamurthi, J. Miner, Mater. Charact. Eng. 2 (2014) 308–318.
[12] Wei Yu, Tong-lai Zhang, Jian-gue Zhang, eujianRren, Yan-horg Liu, J. Mol. Stru. 4 (2006) 255–260.
[13] Mary Anjalin, N. Kanagathara, A.R.Baby Suganthi, Mater. Today 33 (2020) 4751–4755.
[14] Rekha Kumari, Raviteja Seera, Arnab De, Rajeev Ranjan, N. Tayur, Guru Row, Cryst. Growth Des. 19 (2019) 5934–5944.
[15] J. Wiliams, Am. Chem. Soc. Symp. Ser. 233 (34) (1984) 712.
[16] S. Leela, K. Ramamurthi, G. Bhagavannarayana, Spectrochim. Acta part A 74 (2009) 78–83.
[17] A. Subashini, R. Kumaravel, S. Leela, H. Stoeckli-Evans, D. Sastikumar, K. Ramamuthi, Spectrachim. Acta A 78 (2011) 935–941.
[18] C.K. Lakshamana Perumal, A. Arulchakkaravarthi, N. Prajesh, P. Santhanaraghavan, Y.C. Huang, M. Ichimura, P. Ramasamy, J. Cryst. Growth 240 (2002) 212–217.
[19] L. Jothi, R. Sakunthaladevi, J. Eng. Res. Appls. 10 (2020) 13–16.
[20] Nimmy L. Johna, Lija K. Joya, M.Saravana Kumara, S.S. Shaijuna, A. Subashini, D. Sajana, Mol Smulat. 44 (2018) 40–54.
[21] M.S. Pandian, et al., Mater. Res. Bull. 47 (2012) 826–835.
[22] BrukerSMART, SAINT, SADABS, Bruker AXS GmbH, Karisruhe, Germany, 2001.
[23] J. Burgess, J. Fawcett, D.R. Russell, S.R. Gilani, V. Palma, Acta Cryst. C55 (1999) 1707–1710.
[24] B. Kaitner, G. Pavlovic, Acta Cryst. C51 (1995) 1875–1878.
[25] G.Y. Yeap, S.B. Teo, H.K. Fun, S.G. Teoh, Acta Cryst. C49 (1993) 1396–1398.
[26] L. Jothi, K. Ramamurthi, Indian J. Sci. Technol. 4 (2011) 666–669.
[27] William Kemp, Organic Spectroscopy, third ed., ELBS, Palgrave Macmillan, 1993.
[28] J. Coates, Interpretation of Infrared Spectra – A Practical Approach, John Wiley & Sons Ltd, Chichester, 2000.
[29] J.R. Dyer, Applications of Absorption Spectroscopy of Organic Compounds, Prentice – Hall of India, New Delhi, 1994.
[30] L. Jothi, G. Vasuki, R. Ramesh Babu, K. Ramamurthi, Optik 125 (2013) 2017–2021.
[31] A. Shanthi, C. Krishnan, P. Selvarajan, J. Cryst. Growth 393 (2014) 7–12.
[32] T.Kishore Kumar, S. Janarthanan, S. Pandi, M.Victor Antony Raj, J. Kanagalakshmi, D.Prem Anand, J. Miner. Mater. Charact. Eng. 9 (2010) 961–972.
[33] S. Leela, T.Deepa Rani, A. Subashini, S. Brindha, R.Ramesh Babu, K. Ramamurthi, Arabian J. Che. 88 (2014) 1–8.
[34] S.A. Begum, M. Hossain, J. Podder, J. Bangladesh Acad. Sci. 33 (2009) 63–70.
[35] S. Akilandeswari, L. Jothi, Kaushik Pal, M. Abd Elkodous, S. Gharieb, E. Sayyad, J. Clust. Sci. (2020) 1–10.
[36] K.J. Arun, S. Jayalekshmi, J. Miner, Mater. Charact. Eng. 8 (2009) 635–646.
[37] R. Sakunthaladevi, L. Jothi, J. Miner, Mater. Charact. Eng. 8 (2020) 133–148.
[38] P. Paramasivam, M. Arivazhagan, C. Ramachandra Raja, Indian J. Pure Appl. Phys. 49 (2011) 394–397.
[39] N.J. Turro, Molecular Photochemistry, Benjamin, New York, 1965.
[40] K. Biemann, Tables of Special Data For Structure Determination of Organic Compounds, Springer Verlag, Berlin Heidelberg, 1989.
[41] A. Aravindan, P. Srinivasan, Cryst. Res. Technol. 11 (2007) 1097–1103.
[42] Aamir Shahzad, Gottfried Kohler, Martin Knapp, Erwin Gaubitzer, Martin Puchinger, Michael Edetsberger J. Transl. Med. 7 (1) (2009) 1–6 99.
[43] S.K. Kurtz, T.T. Perry, J. Appl. Phys. 39 (1968) 3798–3813.
[44] K. Sathyamoorthy, P. Vinothkumar, J. Irshad Ahamed, P. Murali Manohar, M. Priya, Jinghe Liu, J.Cryst. Growth 487 (2018) 96–103.
[45] S. Janarthanan, R. Sugaraj Samuel, S. Selvakumar, Y.C. Rajan, D. Jayaraman, J. Mater. Sci. Technol. 27 (2011) 271–274.
[46] J. Uma, V. Rajendran, Int. J. Comput. Appl. 30 (2011) 8–10.
[47] H.X. Cang, W.D. Huang, Y.H. Zhou, J. Cryst. Growth 192 (1998) 236–242.
[48] G. Socrates, Infrared Characteristic Group Frequencies, Wiley Inter science, Chichester, 1980.
[49] S. Gunasekaran, G. Anand, S. Kumaresan, S. Kalainathan, Adv. Appl. Sci. Res. 2 (2011) 550–557.
[50] R. Sakunthaladevi, L. Jothi, in: Proc. Inter. Conf. Mat. Spect., Tamilnadu, India, 2019.
[51] Martin Dhas, S. Natarajan, Opt. Commun. 278 (2007) 434–438.
[52] M.S. Kajamuhideen, K. Sethuraman, K. Ramamurthi, P. Ramasamy, J. Cryst. Growth 483 (2018) 16–25.
[53] J. Gubicza, A. Juhasz, P. Tasnh, P. Arat, G. Voros, J. Mater. Scien. 31 (1996) 3109–3114.
[54] E.M. Onitsch, Mikroskopie 2 (1947) 131–151.
[55] M. Hanneman, Metall. Manchu. 23 (1941) 135–140.
[56] R. Sakunthaladevi, L. Jothi, Shanlax International Journal of Arts, Science and Humanities, 4 (2017) 49–52.
[57] N. Vijayan, R. Ramesh Babu, R. Gopalakrishnan, P. Ramasamy, W.T.A. Harrison, J. Cryst. Growth 262 (2004) 490–498.
[58] N. Vijayan, R.Ramesh Babu, M. Gunasekaran, R. Kumaresan, R. Gopalakrishnan, P. Ramasamy, C.W. Lan, J. Cryst. Growth 249 (2003) 309–315.
[59] G. Anandha Babu, P. Ramasamy, J. Cryst. Growth 310 (2008) 3561–3567.
[60] M.Gulam Mohamed, K. Rajarajan, M. Vimalan, J. Madhavan, P. Sagayaraj, Arch. Appl. Sci. Res. 2 (3) (2010) 81–93.
[61] T. Vela, P. Selvarajan, T.H. Freeda, J. Miner, Mater. Charact. Eng. 10 (2011) 959–972.
[62] M. Vimalan, A. Cyrac Peter, T. Rajesh kumar, C. Jayasekaran, J. Packiam Julius, P. Sagayaraj, Arch. Phys. Res. 1 (2010) 94–102.
[63] S. Boomadevi, R.D. Dhanasekaran, J. Cryst. Growth 261 (2004) 70–76.
[64] V.A. Hiremath, A. Venkatraman, Bull. Mater. Sci. 26 (2003) 391–396.
[65] R. Sankar, C.M. Raghavan, M. Balaji, R. Mohan Kumar, R. Jayavel, Cryst. Growth Des. 7 (2007) 348–353.
[66] S. Suresh, A. Ramanand, P. Mani, K. Anand, Arch. Appl. Scien. Rese. 2 (2010) 119–127.
[67] S. Suresh, A. Ramanand, D. Jayaraman, P. Mani, K. Anand, Inter. J. Chem. Tech. Res. 3 (2011) 122–125.